

# A Portable Electrochemical Measurement Platform for Wearable-Flexible Sweat Sensors

**DOI:**
10.1109/sas58821.2023.10254071

**Document Version**
Accepted author manuscript

# A Portable Electrochemical Measurement Platform for Wearable-Flexible Sweat Sensors

Mahdi Saleh[1], Zixin Wang[1], John C. Batchelor[2], Alexander J. Casson[1]
[1] Department of Electrical and Electronic Engineering, University of Manchester, Manchester, M13 9PL, UK
[2] School of Engineering, University of Kent, Kent, CT2 7NZ, UK
mahdi.saleh@manchester.ac.uk

***Abstract*—This paper presents the design, implementation, and testing of a portable electrochemical measurement platform that can perform amperometric, voltametric, and impedance measurements required by different wearable-flexible sweat sensors. These sensors are gaining increasing interest in the domain of healthcare monitoring due to their advantages including low-cost, high sensitivity, and non-invasive operation. The proposed platform is composed of a high-sensitivity Electrochemical Front End (EFE) controlled by a low-power microcontroller (MCU) which is suitable for long-lasting Internet-of-Things (IoT) enabled applications. The implemented prototype provides real-time continuous electrochemical measurements of a novel screen-printed sweat sensor composed of a flexible substrate with several transducing elements targeting different sweat components; $Na^+$, $K^+$, pH, and lactate enzyme. The experimental evaluation presented in this paper demonstrates the effectiveness of our proposed sensing solution for measuring key biomarkers continuously and with high sensitivity.**

***Keywords—electrochemical sensing, flexible sensors, instrumentation, sweat sensors, wearable sensors***

## I. Introduction

The use of portable, wearable, and flexible sensors is rapidly rising in a wide range of healthcare-monitoring and diagnostic applications due to their advantages such as low-cost, autonomous operation, and high sensitivity [1]. These applications include challenging topics such as detecting skin cancer based on electromagnetic waves [2] and monitoring glucose in the blood using in-ear non-invasive PPG sensors [3]. Wearable sensors for detecting Chemical or Biological agents, known as biosensors, can provide continuous monitoring of biomarkers in real time. They are composed of transducing elements that react to specific biological analytes through selective chemical reactions. The results of these reactions are converted to electrical signals that can be processed and measured to estimate the concentration of the measurand. This conversion is done through electrochemical sensing techniques such as potentiometric, amperometric, and impedimetric methods.

In the literature, different types of biosensors have been proposed for a wide variety of applications including vital sign monitoring and physiological monitoring [4]. Sweat sensors are biosensors that can be embedded in wearable devices designed for continuous healthcare monitoring. They are usually designed using flexible substrates holding ion-selective electrodes. For instance, Nyein et al. [5] presented a flexible sweat-sensing patch integrating a spiral-patterned microfluidic component with a set of ion-selective electrodes and an electrical impedance-based sweat rate sensor.

Electrochemical sensing techniques (amperometric and potentiometric) are the main methods used to analyze sweat biomarkers. This is related to their ability to target specific analytes through highly sensitive chemical reactions that produce identifiable electrical signals [6]. They are characterized by several essential features for biosensing applications such as high sensitivity, precision, selectivity, robustness, minimal sample volume requirements, fast analysis rate, and compatibility with biological fluids. These properties allow them to be used in many challenging sensing applications such as for measuring MicroRNAs (miRNAs) in blood [7], monitoring cortisol and glucose levels in sweat [8], and detecting new viral and infectious diseases [9] [10]. In addition to these technical properties, electrochemical sensors have other desired properties such as being low-cost, simple to manufacture and operate, capable of miniaturization, and portable; can be embedded in compact wearable monitoring devices [11].

The electrical circuits required to measure the sweat components using different electrochemical techniques were studied by many researchers with the aim to create a high-sensitivity, low-power, and multichannel measurement solution for wearable sensors. For instance, [12] proposed a multichannel measurement platform based on four instrumentation amplifiers connected to a single Analog-to-Digital Converter (ADC). The measurement capabilities of such systems are limited to performing Open Circuit Potential (OCP) measurements. In addition to OCP measurements, the system presented in [5] added the capability of performing impedance measurements using the high-precision impedance converter system AD5933 provided by Analog Devices (AD) [13]. In [14], the authors used a trans-impedance amplifier circuit for the measurement of lactate levels and non-inverting amplifiers for the potentiometric measurement of the pH levels. In [15], separate potentiometric circuits based on differential amplifiers, and amperometric circuits based on trans-impedance amplifiers were used for performing in situ perspiration analysis. In addition to these custom circuits, many studies, such as [16], [17], relied on potentiostat chips such as the LMP91000 provided by Texas Instruments (TI) [18].

In this work, we propose a unified, portable, and compact electrochemical measurement platform that can perform potentiometric, amperometric, and impedimetric measurements to interface with different types of flexible sensors. Based upon the AD5941 from Analog Devices, our platform allows a wide range of different measurement approaches to be applied, such that it can be used in the detection of many different biomarkers. For demonstration in this paper, the sensor evaluated here is a novel flexible sweat sensor targeting sweat-based analytes. The initial version of this sensor was introduced in our previous work presented in [19]. The sensor was able to measure sweat-based elements ($Na^+$, $K^+$, and pH) in a non-invasive and continuous manner. However, its measurements were performed using the OctoStat30 potentiostat and were limited to OCP. The portable electrochemical measurement platform proposed in this work provides potentiometric and amperometric

measurements, in a small, portable, and low-power form factor. Note that the new sensor prototype presented in this paper includes an additional sensing element for estimating the concentration of the lactate enzyme. The proposed measurement system includes a high-sensitivity Electrochemical Front End (EFE) controlled by an ultra-low power microcontroller (MCU). The experimental evaluation presented in this paper demonstrates its effectiveness in measuring all of the required sensing elements with high accuracy and precision.

The remainder of this paper is organized as follows. Section II presents the proposed system design and describes the structure of the flexible sweat sensor. Section III discusses the physical implementation of the measurement PCB and the MCU firmware development. Section IV presents the experimental evaluation and discusses the results. Finally, the conclusion and future work are provided in Section V.

## II. Proposed System Design

This section describes the proposed system components including the flexible sweat sensor, instrumentation circuit, and microcontroller.

### A. Proposed flexible sweat sensor

Our proposed sweat sensor is composed of a flexible substrate holding $Na^+$, $K^+$ ion-selective electrodes, pH, and lactate sensing elements (see Fig. 1). It operates based on the electro-chemical sensing principle which uses three types of electrodes: Working Electrode (WE) (also known as the Sensing Electrode (SE)), Reference Electrode (RE), and Counter Electrode (CE).

The first three sensing elements ($Na^+$, $K^+$, and pH) were printed using a semi-automatic screen printer on 50 µm Polyethylene naphthalate (PEN) films. Carbon ink (Dupont 7102) was screen printed as the working and counter electrodes and cured at 120 °C for 10 minutes. Ag/AgCl ink (Dupont 5880) was printed as the reference electrode with the same curing conditions. A UV-curable dielectric ink (Dupont 5018) was applied to constitute the boundary of the active sensing chamber, and the complete electrode array was UV cured for 15 minutes. The complete sensor fabrication process and the composition of the transducing layers were discussed in detail in our previous study presented in [19]. The results of our previous study demonstrated the role of increasing the sensing area of the working electrodes in enhancing the sensitivity of the sensing elements.

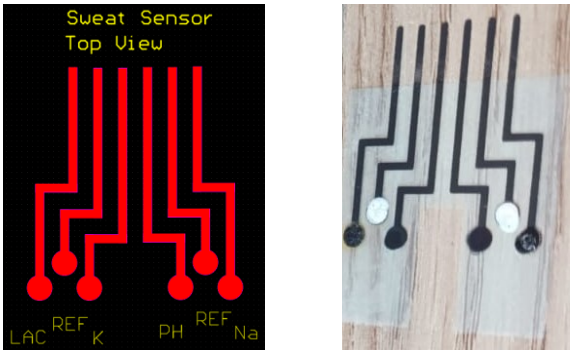


Fig. 1. Proposed flexible sweat sensor. (Left) Schematic design. (Right) Fabricated example. Electrodes from left to right: lactate, reference, $K^+$, pH, reference, $Na^+$. The sensing area is 3 mm diameter circles, and the total size is 2.5 cm x 3.8 cm.

The newly introduced lactate sensing element was made of the carbon working transducer electrode with a mediating layer and an enzyme layer. The mediating layer is made of a tetrathiafulvalene / single-walled carbon nanotube dispersion layer. Subsequently, the mixture of lactate oxidase solution and chitosan/CNT dispersion was drop-casted onto the mediating layer and dried overnight at room temperature.

### B. Proposed electrochemical measurement unit

The elements of our sweat sensor require two types of measurements: OCP and amperometric. OCP is required to measure the first three elements ($Na^+$, $K^+$, and pH) and is applied while not providing any external potential bias; the measured solution is kept in an open-circuit mode where no current is flowing into it. The result of this measurement is the maximum electric potential difference between the RE and the WE electrodes while being immersed in the same solution. The second type of electrochemical measurement required by the fourth sensing element (lactate) is known as amperometric and requires the application of a potential bias while measuring the response current. In addition, the measurement unit should be able to switch between different electrodes to sample all parameters in real time.

Based on the requirements described above, we selected the AD5941 Integrated Circuit (IC) provided by Analog Devices (AD) [20] as a high-precision, ultra-low power, Electro-chemical Front End (EFE) for performing the OCP and amperometric measurements required by our sweat sensor. As shown in Fig. 2, the AD5941 EFE includes a low bandwidth Analog Front End (AFE) loop that can be used to apply the amperometric measurements required to estimate the lactate concentration. The low-power Digital-to-Analog Converter (DAC), potentiostat amplifier, and Low Power Transimpedance Amplifier (LPTIA) are used to apply voltage bias to the sensor (between the CE/RE and SE terminals) and measure the response current.

The first component of the low bandwidth AFE loop is the DAC which provides 12-bit and 6-bit outputs. The 12-bit output $V_{BIAS}$ sets the voltage on CE and RE. The 6-bit output $V_{ZERO}$ sets the voltage on SE. The voltage difference is set between $V_{BIAS}$ and $V_{ZERO}$ programmatically and depends on the requirements of the target biosensor. The second component of this circuit is the LPTIA which converts the current resulting from the chemical reaction into a voltage that can be processed and measured through the high-precision 16-bit Analog-to-Digital Converter (ADC). The value of the internal $R_{TIA}$ is set programmatically and depends on the maximum expected value of the measured current. In many electrochemical sensing scenarios, the generated current is directly related to the concentration of the measurand, and its maximum expected value can be detected via choro-amperometric experiments. Another measurement technique that can be applied using the same circuit is known as Cyclic Voltammetry (CV). It is similar to amperometric measurements in terms of applying a voltage bias and measuring the resulting current, however, it requires incrementing the voltage bias after each measurement and then decrementing it linearly following a triangular function.

For measuring the OCP of the first three sensing elements ($Na^+$, $K^+$, and pH), the AD5941 chip allows for differential voltage measurements through its embedded ADC. The inputs of the ADC can be switched programmatically to different positive and negative input terminals via the embedded input multiplexer.

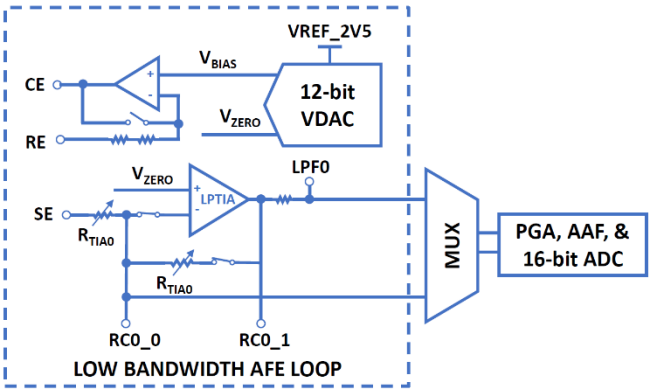


Fig. 2. An electrical schematic of the low bandwidth AFE loop embedded in the AD5941 IC (adapted from AD5941 datasheet [20])

In addition to the amperometric and voltametric measurements, the AD5941 chip can perform impedance measurements using a set of excitation frequencies (up to 200 kHz) using its high bandwidth AFE loop [21]. One major importance of having all these functionalities in a single configurable chip is that it facilitates its mounting to flexible substrates in space-constrained sensing applications. Our platform supports the use of this mode and data collection, although it is not utilized for our current biomarkers under consideration.

The microcontroller selected to interface the AD5941 chip is the MSP430FR5969 provided by Texas Instruments (TI) [22]. It is a 16 MHz MCU with 64 KB FRAM, 2 KB SRAM, and 12-bit ADC. It offers several digital interfaces including SPI, UART, and I2C, and supports different ultra-low-power operation modes. It was selected due to its low power (active mode: approximately 100 µA / MHz) and its ability to interface the AD5941 chip through a high-speed SPI port. The block diagram shown in Fig. 3 describes the connection between the MCU and the EFE and summarizes the structure of our proposed system.

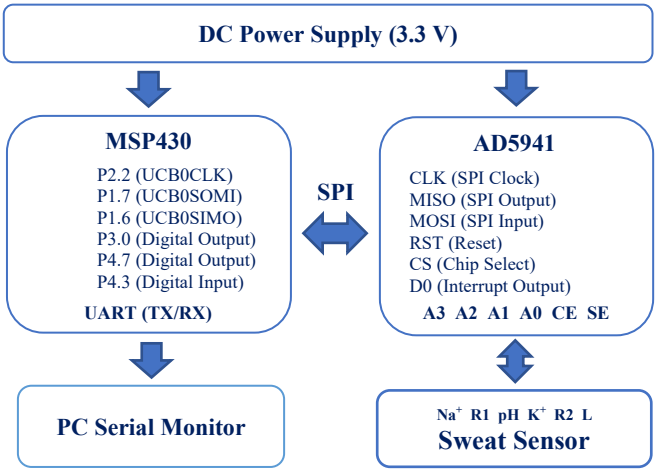


Fig. 3. Block diagram of the main components of our proposed system.

### C. *Properties of the proposed system*

Our proposed system has properties that allow it to effectively interface highly-sensitive biosensors. First, it can perform potentiometric and amperometric measurements that represent the most commonly-used techniques. As described before, this feature is available through the low-bandwidth AFE loop that performs amperometric measurements and through the embedded high-precision ADC. Second, it measures the analytes targeted by our novel flexible sweat sensor. Based on our previous study [19], a sensitivity of around 85 mV/decade (10 – 160 mM) was recorded for the $Na^+$ sensor, 75 mV/decade for the $K^+$ sensor, and 60 mV /decade for the pH sensor. As is shown later in the experimental evaluation section, our system can measure all of the tested concentrations with high accuracy and precision; it shows an average step-change of 28 mV/ 20 mM of $Na^+$, 26 mV/16 mM of $K^+$, and 33 mV/1 pH. The LPTIA measures output current ranging between 50 pA and 3 mA. In our experiments, the system detected an increase of 0.2 µA / 10 mM of lactate concentration using amperometric measurements. The AD5941 is characterized by its low current consumption ranging between a few mico amperes to tens of milli amperes depending on the active features. In combination with the MSP430 MCU, the maximum expected current consumption of the device is in the order of a few milliamperes. However, the exact current consumption depends on several factors including the clock frequency, activated internal modules, and mode of operation.

## III. Physical Implementation

This section describes the physical implementation of the circuit PCB and the development of the required firmware.

### A. *PCB Implementation*

The PCB design of the measurement circuit was implemented using Altium Designer and manufactured via a dual-layer FR4-based PCB. All of the circuit components had surface-mount packages and the ICs were selected as Quad Flat No-lead (QFN). This facilitates their mounting on a completely flexible substrate in the future implementation of the system. The flexible sweat sensor was connected to the measurement circuit using an FFC/FPC connector (FD9 series) as shown in Fig. 4. This offers the sensor a vibration-resistant connection with a bottom contact and a positive locking mechanism.

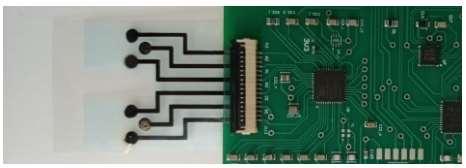

Fig. 4. Proposed flexible sweat sensor connected to the implemented multi-sense PCB via the FD9 connector.

### B. *Firmware development*

The MSP430 firmware required to interact with the AD5941 chip was developed using the C library provided by AD [23]. Initially, we started developing the code using the electrochemical evaluation kit EVAL-AD5941 [24] which facilitates access to the AD5941 chip. Since the firmware examples provided by AD are limited to the ADuCM3029 MCU (AD) and the NUCLEO-F411RE board (ST), we created a set of new C functions that can allow porting the provided examples to fit the MSP430 MCU. Our developed firmware code is available online in a public GitHub repository [25]. The main custom functions developed to communicate with the AD5941 chip via the SPI port performed the following tasks: reading and writing specific bytes via the SPI port, configuring the SPI parameters, configuring the system clock, performing a micro-second-based delay, configuring the interrupts handler, and configuring the UART-based communication port.

## IV. Experimental Evaluation

This section describes the experiments performed to evaluate the implemented circuit's performance.

### A. Experimental setup

Experiments were performed in indoor laboratory conditions using standard testing solutions prepared with deionized water with different NaCl and KCl concentrations for the analytes measurements. Mcllvaine buffer was prepared for pH standard testing solutions. For lactate testing, 0–25 mM lactic acid solution in increments of 5 mM was prepared using lactic acid and deionized water. The measurements were monitored and stored using a PC-based serial monitor application (Tera Term) at a baud rate of 57600 bits/s. The powering of the circuit, debugging of the code, and reporting of the measurements were done through the MSP-FET emulation development tool provided by Texas Instruments (TI) [26]. The connections used to connect our implemented PCB to the MSP-FET development kit are listed in TABLE I.

TABLE I. Experimental Setup – PCB/MSP-FET Connections

| PCB | MSP-FET (TI) | Notes |
|---|---|---|
| VIN (AD5941) | PIN2 (VCC_TOOL) | 3V3 Power |
| VIN (MSP430) | PIN2 (VCC_TOOL) | 3V3 Power |
| GND | PIN9 (GND) | GND |
| MSP430 TX | PIN12 (UART_TX) | UART Port |
| MSP430 RX | PIN14 (UART_RX) | UART Port |
| MSP430 TCK | PIN7 (TCK) | Firmware Flashing |
| MSP430 TDIO | PIN1 (TDO/TDI) | Firmware Flashing |

In each test, the measurements were recorded after dropping a sample solution of a different concentration, using a micropipette, to cover the area containing the relevant working and reference electrodes. In the first three tests ($Na^+$, $K^+$, and pH), the measurements were recorded for 2 minutes and were sampled at a rate of 1 measurement per second. A photo of the measurement setup showing the measured sample covering the area between a reference electrode and a sensing electrode is shown in Fig. 5.

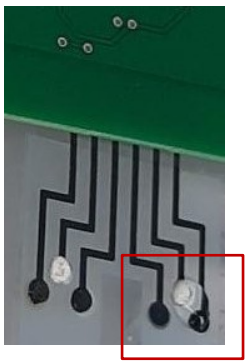

Fig. 5. Photo of the sensor showing one of the measured samples covering the area between one reference electrode and one sensing electrode

### B. Measurement of $Na^+$, $K^+$, and pH

OCP measurements were applied to measure $K^+$, $Na^+$, and pH levels. The AD5941 chip was programmed to apply differential voltage measurements and ADC conversions while switching its positive and negative input terminals to match the working and reference electrodes used in each experiment. The results of the first experiment targeting the $Na^+$ sensor are plotted in Fig. 6 and summarized in TABLE II. The results showed a significant difference between the averages of the OCP measurements obtained relative to different $Na^+$ concentrations (20, 40, and 80 mM); an average step-change of 28 mV for an increase in 20 mM of concentration. In addition, the results showed high stability of the measurements with very low standard deviation values ranging between 0.18 and 1.14 mV (relative standard deviation ranging between 0.15% and 1.31%).

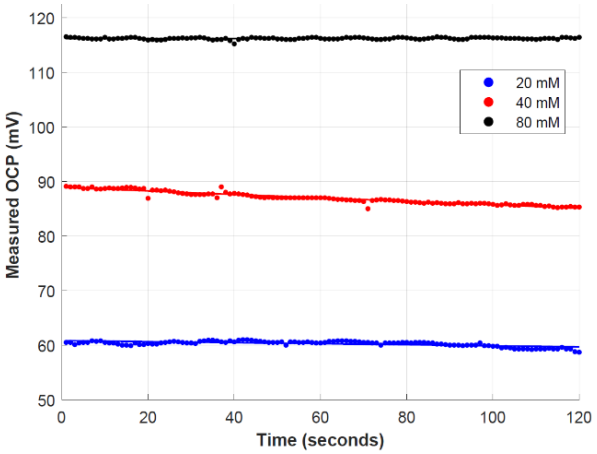


Fig. 6. Measured OCP (mV) vs. different $Na^+$ concentrations (mM)

TABLE II. Summary of OCP Measurements ($Na^+$)

| | Measured OCP (mV) | | |
|---|---|---|---|
| | **20 mM** | **40 mM** | **80 mM** |
| **Average** | 60.3 | 87.0 | 116.2 |
| **Standard deviation** | 0.50 | 1.14 | 00.18 |
| **Maximum** | 61.0 | 89.1 | 116.5 |
| **Minimum** | 58.7 | 85.0 | 115.2 |
| **Dynamic range** | 02.3 | 04.1 | 001.3 |

After completing the experiments of the $Na^+$ sensor, a similar testing procedure was followed to evaluate the $K^+$ sensor. Three different concentrations of the $K^+$ solution were evaluated (16, 32, and 64 mM) via OCP measurements. The results of the $K^+$ sensor tests are plotted in Fig. 7 and summarized in TABLE III.

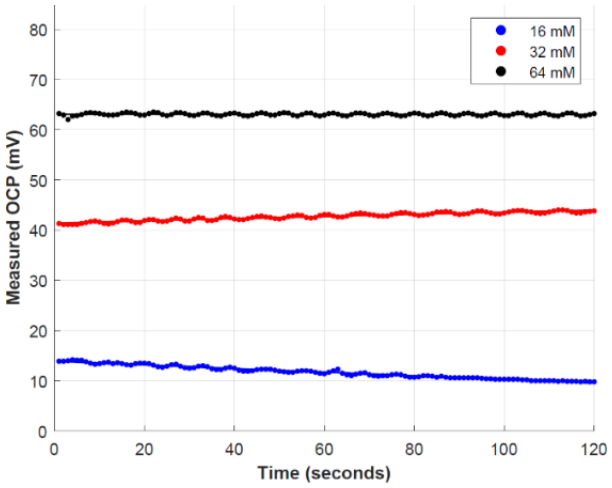


Fig. 7. Measured OCP (mV) vs. different $K^+$ concentrations (mM)

The average step change in the mean value of the OCP measurements is around 26 mV per increase of 16 mM of concentration. All results showed high stability demonstrated by very low standard deviation values ranging between 0.25 and 1.27 mV (relative standard deviation ranging between

0.39% and 10.85%). It was noted that the stability of the measurements increased directly with the concentration of the tested solution.

TABLE III. SUMMARY OF OCP MEASUREMENTS ($K^+$)

| | Measured OCP (mV) | | |
|---|---|---|---|
| | **16 mM** | **32 mM** | **64 mM** |
| **Average** | 11.7 | 42.7 | 63.0 |
| **Standard deviation** | 1.27 | 0.80 | 0.25 |
| **Maximum** | 14.2 | 44.0 | 63.5 |
| **Minimum** | 09.8 | 41.1 | 62.0 |
| **Dynamic range** | 04.4 | 02.9 | 01.5 |

The pH sensor was also evaluated using OCP measurements obtained through three different pH levels (3, 4, and 5). The results of the pH sensor tests are plotted in Fig. 8 and summarized in TABLE IV. As shown in the results, all measurements showed high stability with low standard deviation values ranging between 2.41 and 7.37 mV (relative standard deviation ranging between 1.94% and 9.2%). The three results showed an average step-change of around 33 mV per change of 1 pH level.

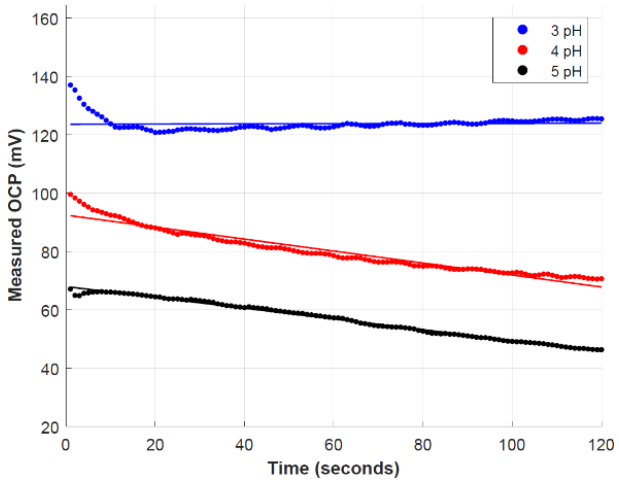


Fig. 8. Measured OCP (mV) vs. different pH levels

TABLE IV. SUMMARY OF OCP MEASUREMENTS (PH)

| | Measured OCP (mV) | | |
|---|---|---|---|
| | **3** | **4** | **5** |
| **Average** | 123.8 | 80.1 | 56.8 |
| **Standard deviation** | 02.41 | 7.37 | 6.45 |
| **Maximum** | 137.1 | 99.6 | 67.2 |
| **Minimum** | 120.8 | 70.6 | 46.4 |
| **Dynamic range** | 016.3 | 29.0 | 20.8 |

### *C. Measurement of lactate*

The lactate measurement experiment was performed in two steps. First, Cyclic Voltammetry (CV) was applied to detect the suitable oxidation potential range for the reaction. Then, a single-step chrono-amperometry measurement was carried out to detect change measured as a function of time, after an input pulse was given. The absolute values and rate of decay then provide information on the amount of lactate present.

A voltage bias of 400 mV was applied between the sensor and reference/counter electrodes through the low bandwidth AFE circuit included in the AD5941 chip. The tests were performed using samples of three lactate concentrations of 0, 10, and 20 mM. Initially, as expected, the current showed a sharply-decreasing trend and then stabilized at a certain value representing the measured lactate concentration (see Fig. 9). The slope of the current decay decreases with increasing lactate concentration. To avoid measuring the decay rate directly, we followed a consistent protocol that can be applied automatically in the MCU firmware to extract a single current value representing the lactate concentration. First, we recorded 150 measurements after drying the electrodes and adding a new sample to them. The average of the last 50 measurements is calculated and used to estimate the lactate concentration. The last 50 measurements obtained from these tests are plotted in Fig. 10 and summarized in TABLE V.

As shown in the results, the current measurements showed an average change of 0.3 µA when the lactate concentration increased from 0 mM to 10 mM and an average change of 0.1 µA when the lactate concentration increased from 10 mM to 20 mM. The measurements were stable with very low standard deviation values ranging between 0.01 and 0.03 µA (relative standard deviation between 0.033% and 0.102%).

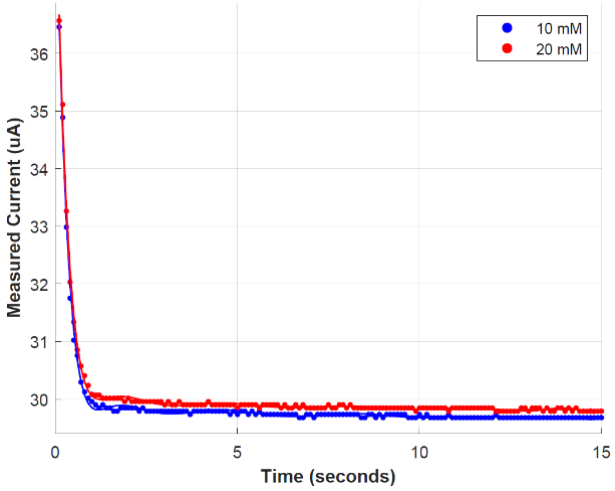


Fig. 9. Current (µA) vs. different lactate concentrations (0 – 15 seconds)

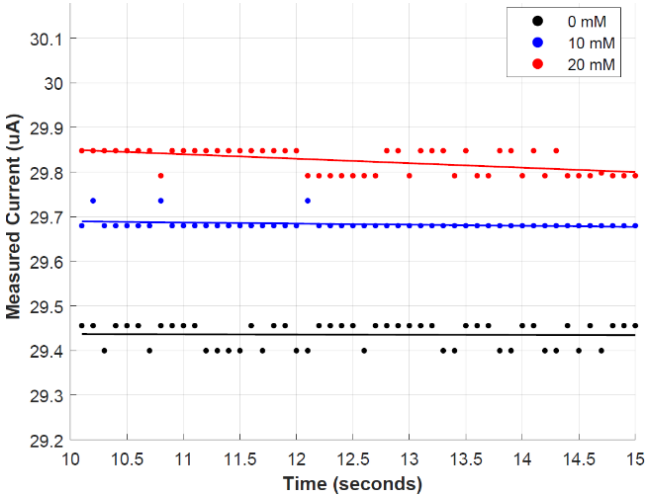


Fig. 10. Current (µA) vs. different lactate concentrations (10 - 15 seconds)

It is important to note that the sensitivity of the lactate sensor is related to its design and could be enhanced by increasing the sensing area of the electrodes. These results demonstrate the effectiveness of our proposed measurement platform to sense current variations representing small changes in lactate concentrations.

TABLE V. SUMMARY OF CURRENT MEASUREMENTS (LACTATE)

| | Measured Current (µA) | | |
|---|---|---|---|
| | **0 mM** | **10 mM** | **20 mM** |
| **Average** | 29.4 | 29.7 | 29.8 |
| **Standard deviation** | 0.03 | 0.01 | 0.03 |
| **Maximum** | 29.5 | 29.7 | 29.9 |
| **Minimum** | 29.4 | 29.7 | 29.8 |
| **Dynamic range** | 0.06 | 0.06 | 0.06 |

We performed a set of experiments to evaluate the power consumption of our proposed system in different settings. The current consumption was measured using the Keysight E6312A power supply which powered the device via a 3.3 V DC signal. The results are summarized in TABLE VI. The average current reaches 0.65 mA when the system is performing amperometric measurements with an MCU clock frequency of 1 MHz. In this case, the internal sequencer of the AD5941 performs the measurement process allowing it to work in a low-power operating mode. The current increases to 7.18 mA when the system is performing continuous OCP measurements via direct SPI commands with an MCU clock frequency of 16 MHz.

TABLE VI. SUMMARY OF CURRENT CONSUMPTION EXPERIMENTS

| **Experiment** | **MCU Clock Frequency (MHz)** | **Average Measured Current (mA)** |
|---|---|---|
| **OCP 1** | 16 | 7.18 |
| **OCP 2** | 8 | 6.57 |
| **OCP 3** | 1 | 6.01 |
| **Amperometric 1** | 16 | 2.95 |
| **Amperometric 2** | 8 | 2.30 |
| **Amperometric 3** | 1 | 0.65 |

## V. CONCLUSION

The portable electrochemical sensing platform presented in this paper is capable of performing most electrochemical sensing methods required by wearable biosensors including amperometric, voltametric, and impedance measurements. The proposed measurement circuit is controlled by an ultra-low-power microcontroller allowing it to be embedded in long-lasting IoT-enabled sensing applications. The experimental evaluation performed in combination with our novel flexible screen-printed sweat sensor demonstrates the ability of our proposed platform to measure different concentrations of sweat components such as $Na^+$, $K^+$, pH, and lactate. It enables the customizability of a multiplexed electrochemical measurement platform for flexible wearable sensors. The possible future work includes the implementation of the proposed measurement circuit on a flexible substrate and combining its measurements with other body sensors such as temperature, ECG, and accelerometric signals.

## REFERENCES


[1] S. Conti *et al.*, "Hybrid Flexible NFC Sensor on Paper," *IEEE Journal on Flexible Electronics*, vol. 2, no. 1, pp. 4–10, Jan. 2023, doi: 10.1109/JFLEX.2023.3238682.

[2] N. Shafi et al., "A Portable Non-Invasive Electromagnetic Lesion-Optimized Sensing Device for The Diagnosis of Skin Cancer (SkanMD)," IEEE Trans Biomed Circuits Syst, vol. PP, Mar. 2023, doi: 10.1109/TBCAS.2023.3260581.

[3] G. Hammour and D. P. Mandic, "An In-Ear PPG-Based Blood Glucose Monitor: A Proof-of-Concept Study," Sensors (Basel), vol. 23, no. 6, p. 3319, Mar. 2023, doi: 10.3390/s23063319.

[4] S. Ajami and F. Teimouri, "Features and application of wearable biosensors in medical care," J Res Med Sci, vol. 20, no. 12, pp. 1208–1215, Dec. 2015, doi: 10.4103/1735-1995.172991.

[5] H. Y. Y. Nyein et al., "A Wearable Microfluidic Sensing Patch for Dynamic Sweat Secretion Analysis," ACS Sens., vol. 3, no. 5, pp. 944–952, May 2018, doi: 10.1021/acssensors.7b00961.

[6] M. Chung, G. Fortunato, and N. Radacsi, "Wearable flexible sweat sensors for healthcare monitoring: a review," Journal of The Royal Society Interface, vol. 16, no. 159, p. 20190217, Oct. 2019, doi: 10.1098/rsif.2019.0217.

[7] P. Jolly, L. C. C. Wong, A. Miodek, M. A. Lindsay, and P. Estrela, "A simple and highly sensitive electrochemical platform for detection of MicroRNAs," in 2015 IEEE SENSORS, Nov. 2015. doi: 10.1109/ICSENS.2015.7370378.

[8] A. R. Naik et al., "Printed microfluidic sweat sensing platform for cortisol and glucose detection," Lab Chip, vol. 22, no. 1, pp. 156–169, Dec. 2021, doi: 10.1039/D1LC00633A.

[9] L. Dennany and K. Brown, "Electrochemical Sensors for New Challenges," in Encyclopedia of Sensors and Biosensors (First Edition), R. Narayan, Ed., Oxford: Elsevier, 2023, pp. 158–173. doi: 10.1016/B978-0-12-822548-6.00078-9.

[10] J. Monzó, I. Insua, F. Fernandez-Trillo, and P. Rodriguez, "Fundamentals, achievements and challenges in the electrochemical sensing of pathogens," Analyst, vol. 140, no. 21, pp. 7116–7128, Oct. 2015, doi: 10.1039/C5AN01330E.

[11] P. C. Ferreira et al., "Wearable electrochemical sensors for forensic and clinical applications," TrAC Trends in Analytical Chemistry, vol. 119, p. 115622, Oct. 2019, doi: 10.1016/j.trac.2019.115622.

[12] L. C. C. Wong, "A Study of Multichannel Open Circuit Potentiometry in Biosensor Applications," Ph.D. dissertation, Department of Electronic and Electrical Engineering, University of Bath, June 2018.

[13] Analog Devices, "AD5933," https://www.analog.com/en/products/ad5933.html (accessed May 5, 2023).

[14] B. Gil, S. Anastasova, and G. Z. Yang, "A Smart Wireless Ear-Worn Device for Cardiovascular and Sweat Parameter Monitoring During Physical Exercise: Design and Performance Results," Sensors (Basel), vol. 19, no. 7, p. 1616, Apr. 2019, doi: 10.3390/s19071616.

[15] W. Gao et al., "Fully integrated wearable sensor arrays for multiplexed in situ perspiration analysis," Nature, vol. 529, no. 7587, pp. 509–514, Jan. 2016, doi: 10.1038/nature16521.

[16] T. Terse-Thakoor et al., "Thread-based multiplexed sensor patch for real-time sweat monitoring," npj Flex Electron, vol. 4, no. 1, Art. no. 1, Jul. 2020, doi: 10.1038/s41528-020-00081-w.

[17] M. A. Yokus, T. Songkakul, V. A. Pozdin, A. Bozkurt, and M. A. Daniele, "Wearable multiplexed biosensor system toward continuous monitoring of metabolites," Biosensors and Bioelectronics, vol. 153, p. 112038, Apr. 2020, doi: 10.1016/j.bios.2020.112038.

[18] Texas Instruments, "LMP91000 Configurable AFE potentiostat for low-power electrochemical cell monitoring," https://www.ti.com/product/LMP91000 (accessed May 5, 2023).

[19] Z. Wang, A. Alwattar, P. Quayle, J. C. Batchelor, and A. J. Casson, "Effects of Sensor Design on the Performance of Wearable Sweat Monitors," in 2022 IEEE Sensors, Oct. 2022, pp. 1–4. doi: 10.1109/SENSORS52175.2022.9967139.

[20] Analog Devices, "AD5940," https://www.analog.com/en/products/ad5940.html#product-overview (accessed May 5, 2023).

[21] A. G. Dutt, M. Verling, and W. Karlen, "Wearable bioimpedance for continuous and context-aware clinical monitoring," in 2020 42nd Annual International Conference of the IEEE Engineering in Medicine & Biology Society (EMBC), Jul. 2020, pp. 3985–3988. doi: 10.1109/EMBC44109.2020.9175298.

[22] Texas Instruments, "MSP430FR5969," https://www.ti.com/product/MSP430FR5969 (accessed May 5, 2023).

[23] Analog Devices, "AD5940 Firmware Library," https://github.com/analogdevicesinc/ad5940lib (accessed May 5, 2023).

[24] Analog Devices, "EVAL-AD5941," https://www.analog.com/en/design-center/evaluation-hardware-and-software/evaluation-boards-kits/eval-ad5941.html (accessed May 5, 2023).

[25] Non-Invasive-Bioelectronics-Lab (UoM), "Portable-Electrochemical-Sensing, https://github.com/Non-Invasive-Bioelectronics-Lab/Portable-Electrochemical-Sensing (accessed May 5, 2023). Doi: 10.48420/22769780.

[26] Texas Instruments, "MSP-FET," https://www.ti.com/tool/MSP-FET (accessed May 5, 2023).